Available online at www.sciencedirect.com
SCIENCE DIRECT®
ELSEVIER
Journal of Nuclear Materials 321 (2003) 29–39
journal of nuclear materials
www.elsevier.com/locate/jnucmat

Plastic deformation in 316LN stainless steel – characterization of deformation microstructures

T.S. Byun *, E.H. Lee, J.D. Hunn

Metals and Ceramics Division, Oak Ridge National Laboratory, Building 45005, P.O. Box 2008, MS-6151, Oak Ridge, TN 37831, USA

Received 17 January 2003; accepted 18 March 2003

Abstract

The effects of irradiation, test temperature, and strain on the deformation microstructures of a 316LN stainless steel have been investigated using a disk-bend method and transmission electron microscopy. Deformation microstructure changed progressively from a dislocation network dominant to a large stacking fault/twin band dominant microstructure with increasing radiation dose and with decreasing test temperature. Also, an increased strain level enhanced the propensity of deformation twinning. Since the stress was considered to be a key external parameter controlling deformation mechanism in 316LN austenitic stainless steel, the equivalent stress level was estimated for the examined surface of the disk sample. It was possible to categorize the deformation microstructures in terms of the equivalent stress range. A key conclusion is that the austenitic material will deform by forming bands of large stacking faults and twins when the stress exceeds a critical equivalent stress level of about 600 MPa by any of several possible strengthening measures: irradiation, increasing strain level, and decreasing test temperature.

1. Introduction

It is known that applying stress to austenitic stainless steels produces a variety of deformation microstructures, depending on material and testing conditions [1–7]. Tangled random dislocations, dislocation pile-ups, defect-cleared dislocation channels, stacking faults, twins, and martensite particles were found in the deformation microstructures. Test temperature, strain rate, strain, and irradiation hardening are known as important parameters that can affect the deformation mechanism of austenitic stainless steels [8–18]. Among the material properties of austenitic stainless steels, the low stacking fault energy (SFE) is believed to be the one most responsible for changes in deformation microstructure in response to external conditions. Low-SFE materials tend to exhibit a more banded, linear array of dislocations and stacking faults [8,19]. All of these features are related to the dissociation of perfect dislocations into two Shockley partial dislocations, so called leading and trailing partials. The separation of the two partials leaves a stacking fault between them and inhibits cross-slip from forming random dislocation structure [8,19–22].

Since the SFE of 316LN stainless steel is believed to be as low as 10 mJ/m^2 [8,14,23], the perfect dislocations in 316LN stainless steel can easily dissociate into two partials during glide, and a large separation of partials can occur by a small change in material or testing conditions. However, the origin of dramatic changes in deformation mechanism has not been clearly elucidated. In room temperature deformation, radiation-induced strengthening produces large stacking fault/twin band dominant microstructures [1–5]. It was also reported that more stacking faults and twins were observed after deformation at cryogenic temperatures [11–13] or at

* Corresponding author. Tel.: +1-865 576 7738; fax: +1-865 574 0641.
E-mail address: byunts@ornl.gov (T.S. Byun).

0022-3115/$ - see front matter © 2003 Elsevier B.V. All rights reserved.
doi:10.1016/S0022-3115(03)00195-8

high speed [19]. Even just heavy plastic deformation at room temperature produced twinned microstructures [4,13]. The deformation microstructure with large separation of partials and twinning in the irradiated 316LN stainless steel was explained by the reaction between leading partial and radiation-induced Frank loops which produces jogs in the dislocation loops [1–3]. The jogged loop becomes a harder obstacle for the trailing partial to overcome. However, this dislocation–defect interaction model cannot explain twin formation in high-speed deformation [19], which does not alter the defect structures. On the other hand, the low SFE at subzero temperature can be the origin of twinning because the SFE of austenitic stainless steels shows a positive temperature dependence [20]. However, the temperature dependence of SFE is usually small (<0.02 mJ/m^2 °C) in austenitic stainless steels and therefore should not induce a dramatic change in deformation microstructure. In addition, although the radiation effect on SFE is unknown for the austenitic stainless steels, the effect is not believed to be large enough to explain the variety in deformation mechanisms after irradiation [4].

However, all of the above microstructures with large stacking faults and twins were produced under conditions of high stress. In the austenitic stainless steels, the conditions of high stress can be usually achieved at subzero temperatures, and any strengthening methods like irradiation or high strain rate might expand the high stress region in the stress-temperature space. We speculate that there exists a common external parameter controlling the deformation mechanism in those experimental conditions and that the single most important parameter might be the stress because the other parameters can be related to the stress. In the present study, therefore, the deformation microstructures of a 316LN stainless steel are characterized for various testing and irradiation cases and are grouped into three categories in terms of equivalent stress range. The results indicate that the austenitic material deforms by forming large stacking fault/twin bands when the stress reaches a critical equivalent stress level of about 600 MPa regardless of different strengthening methods.

2. Experimental

The test material examined was an AISI 316LN stainless steel with the chemical composition of Fe–16.3Cr–10.2Ni–2.01Mo–1.75Mn–0.39Si–0.009C–0.11N–0.029P (in wt%) [1–3]. Transmission electron microscopy (TEM) disks of 3 mm diameter were punched from 0.25 mm thick cold-rolled sheets. The disks were solution annealed in a vacuum for 30 min at 1050 °C after mechanical polishing. One side of each heat-treated TEM disk was then mechanically polished using 0.1 μm diamond paste and then electrochemically polished to produce a flat and dislocation free surface. The polished surface layer was ion-irradiated and examined by TEM.

Different deformation microstructures were produced by deformation after irradiation with helium ions or by deformation of unirradiated specimens at different temperatures. The polished sides of the TEM disks were irradiated up to 15 dpa (or 20 at.% He) at 200 °C with 360 keV He^+ using a 2.5 MV Van de Graaff accelerator. The ion energy produced maximum helium deposition and displacement damage at a depth of 700–800 nm [7,24,25]. The TEM disks were deformed using a disk bend method [1–3,6,7]. In this method, the polished or irradiated side of a TEM disk is placed facedown onto the circular recess of a die with clamping, and a load is applied to the top of the disk through a tungsten carbide (WC) ball of 1 mm diameter and a rod plunger of 1 mm diameter. The estimated equivalent strain rate was about 3×10^{-3} s^{-1}. The irradiated disk samples were deformed at room temperature (~20 °C) and the unirradiated disk samples were deformed at various temperatures in the range −150 to +400 °C.

To estimate plastic strain at the bottom (polished) surface of the disk, a model has been developed and applied to austenitic and ferritic steels [6,7]. In this method, the surface strain (plastic, equivalent strain) of the bottom side, which is assumed to be the same as the strain in the maximum damage layer below surface, is calculated approximately from the measurements of thickness change and ball-impression size:

$$\varepsilon_S^P = 2\ln\left(\frac{t_0}{t}\right) - 0.2\left(\frac{d_p}{D}\right), \quad (1)$$

where t_0 and t are the thicknesses of the center region of the disk before and after deformation, respectively, and d_p and D are the plastic diameter of the indentation impression by the WC ball and the ball diameter, respectively. The thickness of a disk was measured using two linear variable differential transducers at the top and bottom of the disk. The diameter of the indentation impression was measured in an optical microscope after bending deformation. Note that this model can be valid only for the center region of the disk where TEM observation is made. Detailed test and evaluation procedures can be found in [6]. By the disk bend method, about 10% plastic strain was introduced at the polished and irradiated surfaces of the irradiated disks and about 8% or 15% plastic strain at the polished surfaces of the unirradiated disks. To categorize the deformation microstructures into groups in terms of the stress level, equivalent stresses (in true stress unit) for deformation microstructures were obtained from the uniaxial tensile stress–strain curves in Refs. [26,27] and in unpublished tensile test data at corresponding doses, strains, and test temperatures.

After deformation, about 500–700 nm thick surface layer of the irradiated and deformed disks was removed electrochemically from the irradiated side, to expose the peak radiation damage region for TEM examination. The specimens were then thinned from the unirradiated side until perforation. For the unirradiated disks, the surface removal procedure was omitted. A Philips CM12 electron microscope was used at 120 keV operating voltage for examination of the deformation microstructure.

3. Influence of variables on deformation microstructure

3.1. Influence of irradiation

Figs. 1 and 2 illustrate the deformation microstructures in unirradiated specimens and after irradiation up to 15 dpa (20 at.% He) and deformation to a plastic strain of about 10% at room temperature. In the unirradiated specimen, Fig. 1(a), a dislocation network is dominant, in which tangled dislocations are slightly aligned along the $\{1\,1\,1\}$ easy glide planes. Small stacking fault segments (indicated by 'SF') of $\sim$0.1 μm in width, measuring in the direction of the fringe lines, are also seen in the figure. These stacking fault segments were formed by dissociation of perfect dislocations (Burgers vector $= (a/2)\langle 1\,1\,0\rangle$ type, where $a =$ lattice parameter) into Shockley partial dislocations ($(a/6)\langle 1\,1\,2\rangle$ type). In the deformation microstructure at a low dose of 0.0015 dpa, Fig. 1(b), the activity of ordinary dislocations was still dominant, however, many small stacking fault segments were found. Also, the width of the stacking faults increased up to about 0.5 μm. At 0.015 dpa, Fig. 1(c), the glide dislocations became more confined on $\{1\,1\,1\}$ planes forming pile-ups. Some of the pile-up dislocations were dissociated into Shockley

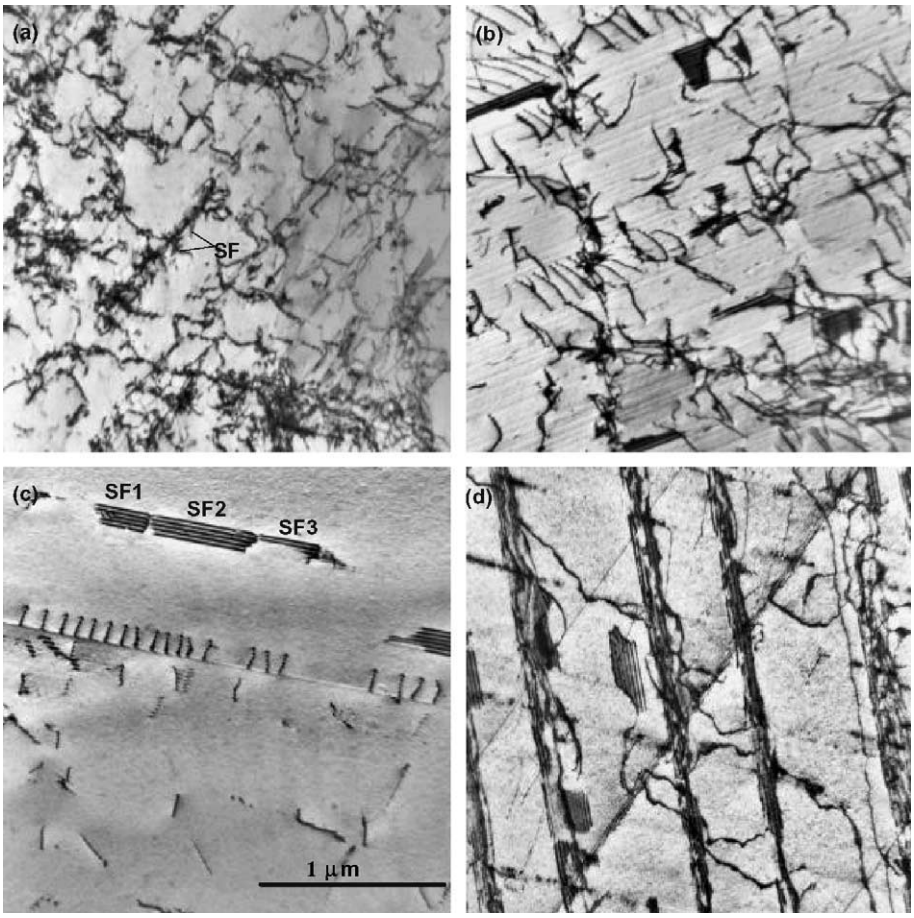

Fig. 1. Deformation microstructures of 316LN stainless steel at a strain of about 10% after irradiation with He ions to doses (a) 0 dpa, (b) 0.0015 dpa, (c) 0.015 dpa and (d) 0.15 dpa. $\vec{Z}$(zone axis) $\approx [1\,1\,0]$ for all pictures; stacking faults are visible on $(1\,\bar{1}\,\bar{1})$ planes. The samples were deformed at room temperature (RT).

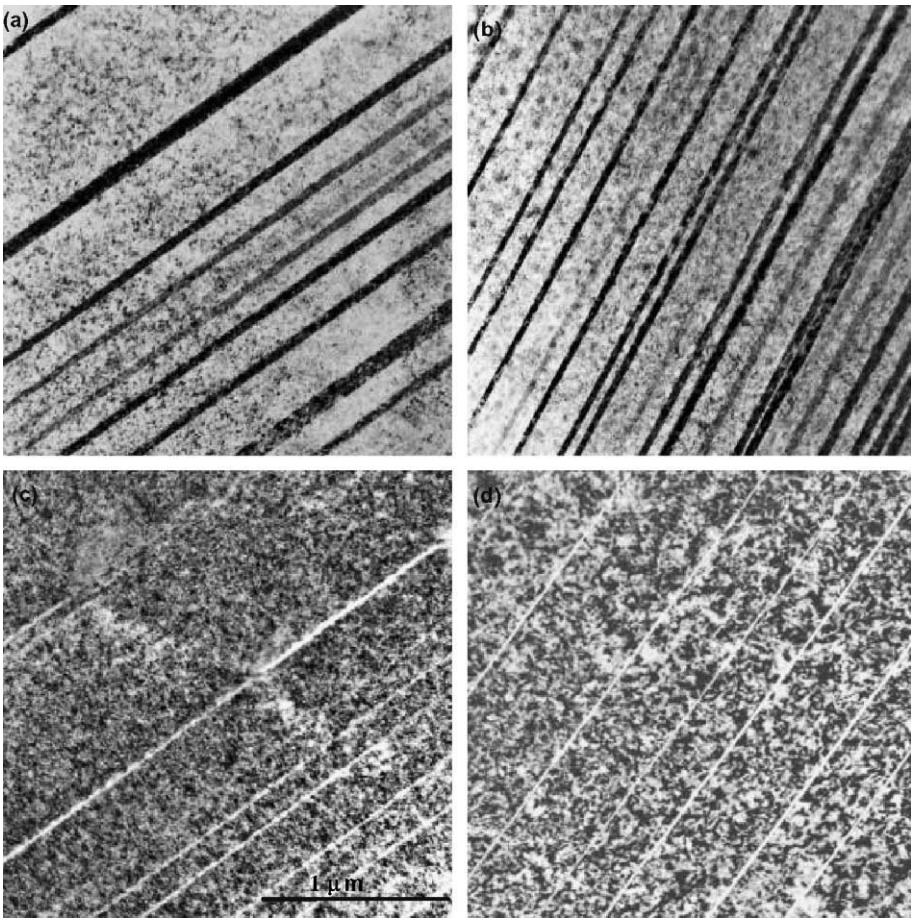

Fig. 2. Deformation twin bands in 316LN stainless steel at a strain of about 10% after irradiation to high doses (a) 1.5 dpa and (b) 15 dpa ($\vec{Z} \approx [1\,0\,0]$); (c) and (d) edge-on views from the samples (a) and (b), respectively ($\vec{Z} \approx [1\,1\,0]$). The samples were deformed at RT.

partials forming three stacking faults in a row on the same plane: SF1, SF2, and SF3.

As the irradiation dose increased, the separation of Shockley partials or the width of stacking faults became larger. At 0.15 dpa, Fig. 1(d), the fringes extended over the whole grain, which appear as long stacking fault strips. Cross-slip seemed to be severely restricted during deformation at 0.15 dpa and dislocation glide occurred mostly on $\{1\,1\,1\}$ slip planes. Patches of stacking fault fringes became evident along the $\{1\,1\,1\}$ glide planes and glide of partials on successive planes formed thin twin layers [1–3]. Some random dislocations are also found in Fig. 1(d). The deformation bands consist of stacking faults/twin layers and perfect and partial dislocations and they formed on at least three slip systems on $\{1\,1\,1\}$ planes.

A dose of 0.15 dpa seemed to be a threshold for the transition of deformation microstructure from glide (by perfect dislocations) dominant to twinning dominant. The separation between leading and trailing partials became infinite or large enough to cover a whole grain, which was usually coincident with twinning dominant. At higher doses, 1.5 and 15 dpa, the propensity for separated partials increased dramatically and the faulted regions on adjacent glide planes began to overlap or glide of partial dislocations occurred on successive planes forming twin bands, which appear as long straight fault ribbons in Fig. 2(a) and (b). The twin bands can be seen as white lines or as black strips depending on the beam conditions in TEM. If being viewed edge-on in TEM, the twin bands appear as white, straight bands of about 10 nm thick, as seen in Figs. 2(c) and 3(d). The white bands at 1.5 dpa have irregular boundaries with the matrix; these bands may be produced by imperfect twinning. Meanwhile, the bands at the highest dose of 15 dpa had clearer boundaries with the matrix. Details on the results of TEM analyses are also presented in the authors' previous reports [1–3].

Overall, the plastic deformation was progressively localized on $\{1\,1\,1\}$ slip planes with increasing dose, as

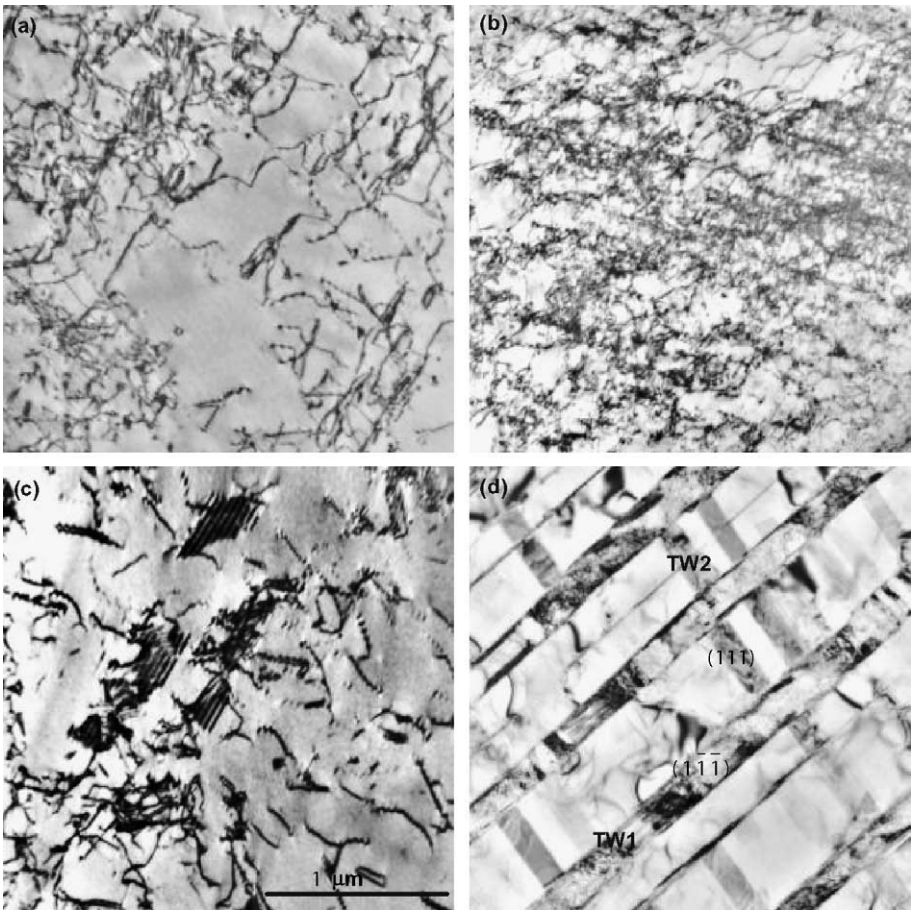

Fig. 3. Deformation microstructures of 316LN stainless steel after disk-bend deformation to a strain of about 15% at different temperatures (a) 400 °C, (b) 200 °C, (c) RT ($\vec{Z} \approx [1\,1\,0]$) and (d) −100 °C ($\vec{Z} \approx [\bar{1}\,1\,3]$).

the ability to cross-slip became increasingly discouraged by the increase of the separation distance of Shockley partial dislocations. Consequently, the deformation microstructure changed from a dislocation network dominant to twin dominant microstructure with increasing radiation dose. It may be an important finding that there exists a transition range of dpa dose in the shift of deformation mechanism from random dislocation networks to twins, in which the separation of partials increases with increasing dose. At room temperature this transition range covered a dose range 0–0.15 dpa.

3.2. Influence of test temperature

A similar transition in deformation microstructure occurred in the unirradiated specimens as the test temperature decreased. Fig. 3(a)–(d) show the temperature dependence of deformation microstructure at a strain of about 15% in the temperature range −100 to +400 °C. At elevated temperatures, 200 and 400 °C, deformation microstructures consisted of tangled dislocations, which indicates that cross-slip occurred during dislocation glide. As the test temperature decreased to room temperature (20 °C), some of the perfect dislocations dissociated into partials during deformation; several stacking faults are found in the dominant dislocation network, and the widths of the stacking faults, or the separations of partials, do not exceed 0.5 μm.

At −100 °C, Fig. 3(d), twin network dominant microstructures were produced at a plastic strain of 15%. The ladder-like feature in the network indicated that parallel twin bands (TW1), or stacking fault bands, initially formed along primary {1 1 1} planes and then additional bands (TW2) formed on other {1 1 1} planes to relieve incompatibility strains at the band-matrix boundaries or to accommodate macroscopic strains. The ladder rung-like secondary twins (TW2) were nucleated at the twin-matrix interfaces and were very thin layers of twins or overlapped stacking faults. Different contrasts within the fringe ribbons indicated that multiple glide of

partial dislocations occurred on successive planes and some of them stopped before arriving at the next twin boundary, which formed small partial dislocation pile-ups.

3.3. Influence of strain level

Fig. 4(a) and (b) are the TEM microstructures after deformation to different strain levels of 8% and 15%, respectively, at −150 °C. Although twins/stacking faults and dislocations are found commonly in both microstructures, twinning became more dominant at the higher strain of 15%. In Fig. 4(a) two long stacking fault strips, or thin twin layers, are formed along with the dislocation tangles and arrays. After straining to 15%, the twin dominant microstructures formed at −150 °C and −100 °C (Fig. 3(d)) look alike; small, thin twins were formed between larger twin bands on primary slip planes, bridging the twin bands on primary planes. Again, in these bridging twins, a few twinning dislocations (marked by dotted arrows), or partial dislocations, were found; the glide of partial dislocations produced different contrasts and slight lateral shift in the fringe lines.

A more detailed investigation of the strain effect was performed for a 316 stainless steel [4]. The deformation mechanism changed gradually from dislocation network to twinning with increasing strain. At a low strain of about 1% the dislocations were primarily in planar arrays and only short stacking fault fringes were frequently visible together with ordinary dislocations. As the strain level increased, the arrays thickened into bands on $\{1\,1\,1\}$ planes, and random, tangled dislocations appeared in the matrix between the bands. At high strains of 50% or so, the twins were very evident with a background structure of dense dislocation tangles [4]. These results also indicate that the macroscopic strain, or stress, can be a key external parameter that controls the deformation mechanism of the 316 stainless steel.

3.4. Differences in twin dominant microstructures

The above results indicate that large stacking fault/twin dominant microstructures were produced by irradiation (Fig. 2) and by reduced deformation temperature (Figs. 3(d) and 4(b)). Although these were classified together as a group of large stacking fault/twin dominant microstructures, it is worth noting that the twin dominant microstructures formed at subzero temperatures of −100 and −150 °C were different from those formed after irradiation. In the irradiated samples the formation of twin bands was strongly confined on a primary slip system, while at least two slip systems operated in the deformation twinning at low temperature. This difference might originate from the difference in defect structures between the two material conditions. Radiation-induced defect microstructures have been characterized in detail after irradiation with He^+ ions [28,29]. Some defect microstructures are presented in Fig. 5 (see Ref. [28] for details). The radiation-induced defects consisted of small black dots (vacancy and interstitial clusters), small faulted Frank interstitial loops ($(a/3)\langle 1\,1\,1\rangle$ type), some unfaulted loops ($(a/2)\langle 1\,1\,0\rangle$ type), and small helium bubbles [28]. In TEM, discernible bubbles began to appear at doses higher than about 0.75 dpa (∼1 at.% He). Both defect cluster number density and size increased with dose and, at about 4 dpa or below, the number density of black dots and loops saturated in the range of $2\text{–}4\times10^{23}$ m^{-3} and the number density of bubbles in a much higher range. It is believed that the radiation-induced defects, except for the helium bubbles, can be removed by dislocation glide and con-

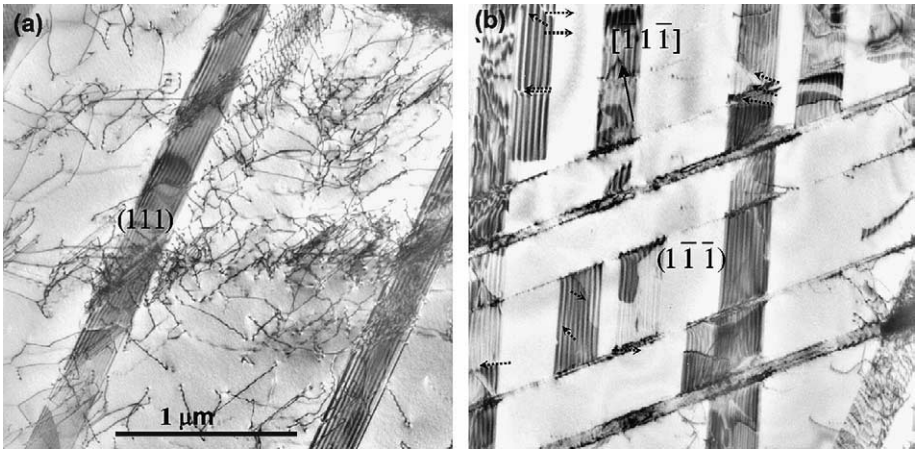

Fig. 4. Deformation microstructures of 316LN stainless steel after disk-bend deformation at −150 °C to different strain levels (a) 8% ($\vec{Z} \approx [\bar{1}\,1\,1]$) and (b) ($\vec{Z} \approx [\bar{1}\,1\,2]$).

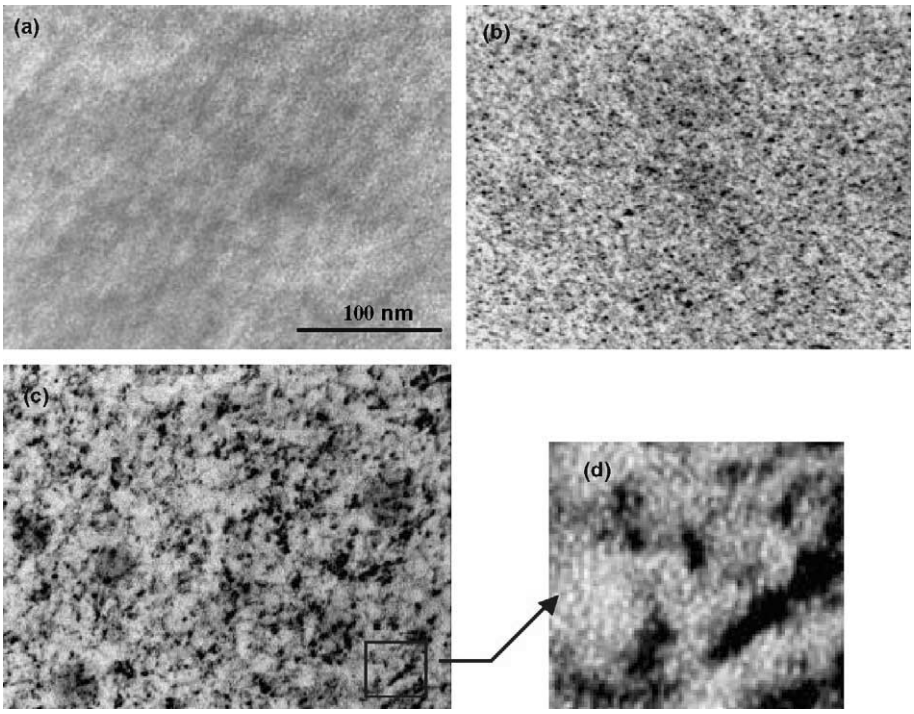

Fig. 5. Defect microstructure after helium irradiation to (a) 0.015, (b) 0.15 and (c) 15 dpa; (d) an enlarged microstructure showing bubbles.

sequently the deformation bands in irradiated materials are softened by the removal of the defects. Therefore, the plastic deformation tended to be localized within the deformation bands, producing parallel and coarse bands on primary slip planes with little strain outside of the bands, as presented in Fig. 2(a)–(d).

In Figs. 3(d) and 4(b), however, the fine twin/stacking fault bands were formed in more than one slip (twinning) system, producing more complex twin networks than in the irradiated samples. The twin/stacking fault bands of different slip systems intercepted each other and produced relatively fine network structures. This indicated that more slip systems had been operating in the unirradiated specimens than in the irradiated specimens. This might be because without the irradiation-induced defects little reduction of strength in the slip bands occurred in the unirradiated specimens. The combination of no defect removal and some strain hardening in the deformation bands might enhance the operation of more twinning sources and glide systems, producing finer twin bands. It is known that the formation of twin networks can increase work hardening in plastic deformation and result in high uniform ductility [26].

Based on these different responses of defect structures to straining, we can anticipate that the softening effect from the removal of defects will be more pronounced in neutron-irradiated materials. Since the removal of defects by earlier dislocation glide enabled easier glide for subsequent dislocation motion, localized deformation bands, or channels, can be formed by successive dislocation glide [30–34]. The number density of helium bubbles in the neutron-irradiated materials might be significantly lower than in the helium-irradiated materials. Helium bubbles, which are shearable but not removable by dislocations, might continue to be effective as barriers to glide after earlier plastic deformation [28,29,35]. Therefore, coarse dislocation channels were formed in the neutron-irradiated 316 stainless steel [4], while formation of twins/stacking faults, which required a higher stress for nucleation than the ordinary dislocation glide, was more favorable in the helium-irradiated 316LN stainless steel. The difference in deformation microstructures after irradiations with helium ions and neutrons was exacerbated at high doses (>1 dpa), where the effect of helium bubbles on hardening becomes significant [35].

In austenitic stainless steels the formation of martensite has been frequently observed during deformation at room temperature or below [5,11,12]. In situ observations on Fe–Ni–Cr stainless steels showed that ε-martensite was formed along with stacking faults, while α-martensite nucleation seemed to be associated with dislocation pile-ups [11,12]. Since in the present study the deformation microstructures formed below room temperature displayed similar microstructures to the

previous observations which showed formation of small martensite particles [11,12] and a weak deflection of electron beam due to magnetized specimens has been experienced during TEM observation, it is believed that a small amount of martensite has been formed in the heavily twinned microstructures: Figs. 3(d) and 4(b). However, the formation of martensite is not considered in detail in the following categorization of microstructures because we believe that the martensite transformation, if any, plays the least important role in plastic deformation among the mechanisms mentioned here [5].

4. Applied stress and microstructural characteristics

As described in Section 2, the plastic strains applied at the surfaces of disks were evaluated using Eq. (1) and corresponding equivalent stresses were obtained from the uniaxial stress–strain curves. In individual grains in a polycrystalline material, the stress state is always complex and triaxial because of mechanical interactions between elastically and plastically anisotropic grains. Even in the surface grains at the center region of a TEM disk, the stress state might be triaxial because it is biaxial macroscopically and there exist mechanical interactions at the grain boundaries except for the free surface of the grain. Therefore, the calculated equivalent stress should be considered as a macroscopic average in the central region of the bottom surface of a disk. In Table 1 microstructure characteristics and corresponding equivalent stresses are listed for various irradiation and test conditions.

In the above deformation microstructures, it was evident that there was a transition region where the separation of Shockley partial dislocations increased from a stress-free equilibrium separation (~10 nm [21,23]), which was invisible in the microstructures, to a large size (>1 μm). Twinning became dominant after the stacking fault size reached the grain size. We believe that a large separation comparable to a grain size was related to a critical condition for the dominance of twinning. Therefore, the separation of Shockley partials, or the size of stacking faults, was a main parameter in categorizing deformation microstructures.

It was possible to group the deformation microstructures of 316LN stainless steel in terms of stress level:

(1) Dislocation tangles were dominant when the equivalent stress was less than about 400 MPa.
(2) Many small, isolated stacking faults, normally less than 1 μm, were found along with dislocations at a stress ranging from about 400 to 600 MPa. This stress range was considered as a transition region in the change of deformation mechanism.
(3) Above 600 MPa, long stacking fault ribbons (>1 μm)/twin bands became dominant. This stress level was believed to be a critical value for twinning in 316 stainless steels.

Table 1
Stress and characteristics of deformation microstructures

Test temperature (°C)	dpa	Equivalent strain (%)	Equivalent stress (MPa)	Characteristics in TEM microstructure
20	0	10	410	Tangled dislocations, small stacking faults
20	0.0015	10	560	Stacking faults, tangled dislocations
20	0.0015	10	560	Stacking faults, pile-up dislocations
20	0.0015	10	560	Pile-up dislocations at grain boundary
20	0.015	10	610	Stacking faults, pile-up dislocations
20	0.015	10	610	Stacking faults, pile-up dislocations
20	0.15	10	670	Long stacking fault strips, isolated stacking faults
20	1.5	10	810	Twins
20	15	10	1010	Twins
400	0	15	310	Tangled dislocations
300	0	15	360	Tangled dislocations
200	0	15	380	Tangled dislocations
100	0	15	650	Tangled dislocations
20	0	15	490	Tangled dislocations, stacking faults (width up to ~0.5 μm)
−50	0	15	660	Twin network, overlapped large stacking faults, dislocations
−100	0	8	630	Twin network, stacking faults, dislocations
−100	0	15	740	Twin network, overlapped stacking faults, dislocations
−150	0	8	790	Twins/large stacking faults, dislocations
−150	0	15	910	Twin network, overlapped stacking faults, dislocations

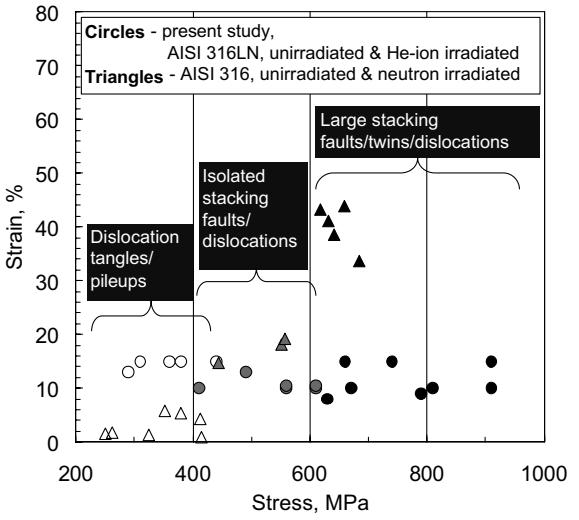

Fig. 6. Deformation microstructures as a function of stress.

The dependence of deformation microstructure on stress is more obvious when the stress/strain regimes of the data are shown as in Fig. 6. In this figure the microstructural data for a reference 316 stainless steel are overlaid on the data for the present 316LN stainless steel. An extensive study on the deformation microstructures has been being carried out for the 316 stainless steel after low temperature (60–70 °C) neutron irradiation up to 0.8 dpa for mapping deformation mechanisms as a function of strain and dose [4]. In Fig. 6 the data for the 316 stainless steel are from tensile samples irradiated up to 0.01 dpa and strained up to about 50%. Data for higher doses were excluded because their microstructures showed dislocation channels [4]. The shift from twinning to channeling after neutron irradiation to high doses is not contrary to the present stress-based characterization because the formation of defect-cleared channels should reduce the flow stress within the channels, which will be explained in detail in an ongoing theoretical approach. In Fig. 6 the boundaries between microstructures are well defined in terms of stress level although the testing and material conditions are different, supporting the suggestion that the stress level determines the deformation mechanism.

In addition to the stress level some changes in SFE and defect structure may affect the details of deformation mechanisms. Existing theoretical models [15,20–22] state that in a stress-free condition the separation distance between Shockley partials (d), or the width of the stacking fault, varies inversely with SFE (γ_{SF}). Among the models the simplest form is one suggested by Cottrell [21,22]:

$$d \approx G(b_p)^2/4\pi\gamma_{SF}, \quad (2)$$

where G is the shear modulus and b_p the magnitude of the Burgers vector of a Shockley partial dislocation. Using typical values for stainless steels: $G = 65.6$ GPa, $b_p = 0.145$ nm, and $\gamma_{SF} = 10$ mJ/m^2, the equilibrium separation would be 17 nm. The size of the large stacking faults covering entire grains is about 1000 times this stress-free equilibrium separation. If assuming that Cottrell's equation holds for the case of stacking fault size reaching the grain size, SFE would be only 0.01 mJ/m^2, an unrealistically low value. Although the SFE can be lowered by changing chemical elements and deformation temperature [20,36,37], very large separation of up to a grain size is unlikely because the effects of those measures on the SFE are limited [36,37]. This confirms again that the formation of stacking faults, and probably twins, cannot be controlled solely by a change in the SFE.

The interactions between partial dislocations and defects have been proposed to cause wider separation of partials [1–3]. The formation of large stacking faults and twins in the test material was explained by an additional strengthening of the trailing partial due to a jog formation by an interaction between radiation-induced Frank loops and the leading partial. This mechanism occurs when the gliding partial intercepts Frank loops on planes different from the glide planes of the partials. Since the jogs at Frank loops with the magnitude of one partial Burger's vector formed by the glide of the first leading partial may not generate stress fields large enough to obstruct the trailing partial, multiple dislocation passages on each Frank loop are necessary to form super jogs that can be obstacles to additional dislocation glide. However, it is uncertain whether the jogged Frank loops, if they are small, can survive the multiple passages of dislocations or if they are unfaulted and cleared by the glide dislocations to form channels [38–41]. Further, the dislocation–defect interaction model cannot explain twin formation in high-speed deformation [19], which does not alter the defect structures. Therefore, the formation of jogs may not be a main cause for the formation of large stacking faults and twins. Rather, we believe that the total strengthening effect from various radiation-induced defects causes the faulted and twinned microstructures.

Finally, although Fig. 6 gives a clear indication that the applied stress correlates to the deformation mechanism, the stresses provided in this study should be viewed with margins. The separation distance of partials, or the size of stacking faults, might be different for different grain orientations and affected by local stress concentrations since the applied stress may be altered by interactions with elastic–plastic properties of grains and with microstructures such as at grain boundaries, annealing twin boundaries, second phases, and dislocation pile-ups. In the microstructural detail, therefore, a large variation in the sizes of stacking faults is expected at

a given applied stress. Even under an applied stress smaller than the twinning stress, a small twin can exist around a stress concentration area because it can be formed by the stress concentration and may stop growing when the stress at a large distance from the stress concentrator becomes too low for further growth.

5. Conclusions

Deformation microstructures of a 316LN stainless steel were investigated as functions of radiation dose or test temperature, and the following conclusions have been drawn:

1. Deformation microstructure changed from a dislocation tangle dominant to a large stacking fault/twin band dominant microstructure with increasing radiation dose and strain or with decreasing test temperature.
2. Since the applied stress was considered to be a key external parameter controlling deformation mechanism, the equivalent stress level was estimated for TEM samples using a model for disk bend deformation.
3. It was possible to categorize the deformation microstructures in terms of the equivalent stress range:
   (1) dislocation tangles were dominant at low equivalent stresses < 400 MPa;
   (2) small, isolated stacking faults less than about 1 μm in width were formed in the stress range from about 400–600 MPa;
   (3) large stacking faults (>1 μm)/twin bands became dominant at stresses > 600 MPa.
4. Ordinary dislocations were found outside of the bands except for the samples irradiated to high doses of 1.5 and 15 dpa.
5. A 316LN austenitic stainless steel will deform by forming stacking fault/twin bands when the equivalent stress reaches a critical level of about 600 MPa due to various strengthening measures such as irradiation, increasing strain, and decreasing test temperature.

Acknowledgements

Research sponsored by the Division of Materials Sciences and Engineering, Office of Basic Energy Sciences, US Department of Energy, under contract no. DE-AC05-00OR22725 with UT-Battelle, LLC.

References

[1] E.H. Lee, T.S. Byun, J.D. Hunn, M.H. Yoo, K. Farrell, L.K. Mansur, Acta Mater. 49 (2001) 3269.
[2] E.H. Lee, M.H. Yoo, T.S. Byun, J.D. Hunn, K. Farrell, L.K. Mansur, Acta Mater. 49 (2001) 3277.
[3] E.H. Lee, T.S. Byun, J.D. Hunn, K. Farrell, L.K. Mansur, J. Nucl. Mater. 296 (2001) 183.
[4] K. Farrell, T.S. Byun, N. Hashimoto, Mapping Flow Localization Processes in Deformation of Irradiated Reactor Structural Alloys, Report for DOE/NERI in Oak Ridge National Laboratory, 2002, ORNL/TM-2002/66.
[5] N. Hashimoto, S.J. Zinkle, A.F. Rowcliffe, J.P. Robertson, S. Jitsukawa, J. Nucl. Mater. 283–287 (2000) 528.
[6] T.S. Byun, E.H. Lee, J.D. Hunn, K. Farrell, L.K. Mansur, J. Nucl. Mater. 294 (2001) 256.
[7] E.H. Lee, T.S. Byun, J.D. Hunn, N. Hashimoto, K. Farrell, J. Nucl. Mater. 281 (2000) 65.
[8] R.W. Hertzberg, Deformation and Fracture Mechanics of Engineering Materials, third Ed., John Wiley, 1989, p. 67.
[9] H.C. Choi, T.K. Ha, H.C. Shin, Y.W. Chang, Scr. Mater. 40 (1999) 1171.
[10] G.T. Gray III, in: M.H. Yoo, M. Wuttig (Eds.), Twinning in Advanced Materials, The Minerals, Metals & Materials Society, 1994, p. 337.
[11] J.W. Brooks, M.H. Loretto, R.E. Smallman, Acta Metall. 27 (1979) 1829.
[12] J.W. Brooks, M.H. Loretto, R.E. Smallman, Acta Metall. 27 (1979) 1839.
[13] P. Müllner, C. Solenthaler, Mater. Sci. Eng. A 230 (1997) 107.
[14] D. Goodchild, W.T. Roberts, D.V. Wilson, Acta Metall. 18 (1970) 1137.
[15] S.M. Copley, B.H. Kear, Acta Metall. 16 (1968) 227.
[16] H.J. Kestenbach, Philos. Mag. 36 (1977) 1509.
[17] J.W. Christian, S. Mahajan, Prog. Mater. Sci. 39 (1995) 1.
[18] M.H. Yoo, Twinning and mechanical behavior, in: J.H. Westbrook, R.L. Fleischer (Eds.), Principles and Practice, Intermetallic Compounds, vol. 3, John Wiley, 2002 (Chapter 21).
[19] M.A. Meyers, K.K. Chawla, Mechanical Behavior of Materials, Prentice-Hall, 1998, p. 264.
[20] L.E. Murr, Interfacial Phenomena in Metals and Alloys, Addision-Wesley, 1975, p. 142.
[21] A.H. Cottrell, An Introduction to Metallurgy, Edward Arnold, 1975, p. 277.
[22] A.H. Cottrell, Theory of Crystal Dislocations, Gordon and Breach Science, 1964, p. 69.
[23] A. Kelly, G.W. Groves, Crystallography and Crystal Defects, J.D. Arrowsmith, 1970, p. 255 (Chapter 8).
[24] M.J. Norgett, M.T. Robinson, I.M. Torrens, Nucl. Eng. Des. 33 (1975) 50.
[25] E.H. Lee, Nucl. Instrum. and Meth. B 151 (1999) 29.
[26] T.S. Byun, K. Farrell, E.H. Lee, J.D. Hunn, L.K. Mansur, J. Nucl. Mater. 298 (2001) 269.
[27] K. Farrell, T.S. Byun, J. Nucl. Mater. 296 (2001) 129.
[28] E.H. Lee, J.D. Hunn, T.S. Byun, L.K. Mansur, J. Nucl. Mater. 280 (2000) 18.
[29] E.H. Lee, J.D. Hunn, N. Hashimoto, L.K. Mansur, J. Nucl. Mater. 278 (2000) 266.
[30] M.S. Wechsler, The Inhomogeneity of Plastic Deformation, American Society for Metals, Metals Park, OH, 1971 (Chapter 2).
[31] J.V. Sharp, Acta Metall. 22 (1974) 449.

[32] J.V. Sharp, Philos. Mag. 16 (1967) 77.
[33] F.A. Smidt, Dislocation Channeling in Irradiated Metals NRL Report 7078, Naval Research Laboratory, Washington, DC 20390, 3 June 1970.
[34] M.J. Makin, J.V. Sharp, Phys. Status Solidi 9 (1965) 109.
[35] J.D. Hunn, E.H. Lee, T.S. Byun, L.K. Mansur, J. Nucl. Mater. 282 (2000) 131.
[36] P.J. Ferreira, P. Müllner, Acta Mater. 46 (1998) 4479.
[37] I.A. Yakubtsov, A. Ariapour, D.D. Perovic, Acta Mater. 47 (1999) 1271.
[38] M. Suzuki, A. Sato, T. Mori, Philos. Mag. 65 (1992) 1039.
[39] J.I. Cole, S.M. Bruemmer, J. Nucl. Mater. 225 (1995) 53.
[40] S.M. Bruemer, J.I. Cole, R.D. Carter, G.S. Was, Mater. Res. Soc. Symp. Proc. 439 (1997) 437.
[41] S.G. Song, J.I. Cole, S.M. Bruemmer, Acta Mater. 45 (1997) 501.